Rev. Adv. Mater. Sci. 41 (2015) 61-71

GRAIN BOUNDARIES AS A SOURCE OF FERROMAGNETISM AND INCREASED SOLUBILITY OF Ni IN NANOGRAINED ZnO

B.B. Straumal[1,2,3], A.A. Mazilkin[1,2], S.G. Protasova[1,2,4], S.V. Stakhanova[3], P.B. Straumal[3,6], M.F. Bulatov[5], G. Schütz[4], Th. Tietze[4], E. Goering[4] and B. Baretzky[2]

[1]Institute of Solid State Physics, Russian Academy of Sciences, Ac. Ossipyan str. 2, 142432 Chernogolovka, Russia
[2]Karlsruhe Institute of Technology, Institute of Nanotechnology, Hermann-von-Helmholtz-Platz 1, 76344 Eggenstein-Leopoldshafen, Germany
[3]National University for Research and Technology "MISiS", Leninsky prospect 4, 119991 Moscow, Russia
[4]Max-Planck-Institut für Intelligente Systeme, Heisenbergstrasse 3, 70569 Stuttgart, Germany
[5]Federal State Research and Design Institute of Rare Metal Industry ("Giredmet"), B. Tolmachevsky lane 5-1, 119017 Moscow, Russia
[6]Institute of Metallurgy and Materials Science, Russian Academy of Sciences, Leninsky prospect 49, 117991 Moscow, Russia

Received: April 03, 2015

Abstract. The dense nanograined ZnO films with various Ni content (between 0 and 40 at.%) were synthesized by the liquid ceramics method. The films with 0, 5, and 10 at.% Ni contain only ZnO-based solid solution with wurzite structure. The peaks of the second phase NiO become visible in the X-rays diffraction patterns above 10 at.% Ni. Using recently published papers, we constructed the dependence of Ni solubility in ZnO on the grain size. The overall Ni solubility drastically increases with decreasing grain size. The influence of the grain boundary specific area s_{GB} on the appearance of ferromagnetism in Ni-doped ZnO has been analysed. The review of numerous papers devoted to the ferromagnetic behaviour of Ni-doped ZnO is given. It has been shown that the main factor controlling such behaviour is the specific grain boundary area s_{GB}. The Ni-doped ZnO is ferromagnetic only if the amount of GBs is high enough and s_{GB} is above a certain crytical value s_{th}. = (1.0±0.2)×10^6 m^2/m^3. It corresponds to the effective grain size of about 4×10^{-6} m assuming that a material is fully dense and grains are equiaxial.

1. INTRODUCTION

The position of the equilibrium lines in the phase diagrams for the nanograined materials can drastically differ from those for the coarse-grained polycrystals or single crystals. For example, in one increases the amount, c, of a second component in a solid solution, a solubility limit is reached at a certain concentration, c_s. Above c_s one can observe the second phase in the bulk, in addition to the solid solution based on the first component. In other words, at $c > c_s$ the diffraction peaks of a second phase appear in the X-rays diffraction (XRD) spectrum and in the electron diffraction pattern in transmission electron microscopy (TEM). If c increases further, only the amount of the second phase increases, but the concentration in the solid solution remains equal to c_s. However, if the second component segregate in the surfaces and interfaces, the total concentration of a second component in a solid solution, c_t, will be higher than the concentration in the bulk, c_v. The difference between c_t and c_v should increase with decreasing grain size (i.e. with an increasing specific area of surfaces and interfaces).

Corresponding author: B.B. Straumal, e-mail: straumal@issp.ac.ru

The difference between c_t and c_v can become measurable if the grain size is small enough. This is due to the fact that XRD (or TEM) can register the diffraction only from the bulk phases. The second component segregated in the thin surface or interface layers remains invisible for XRD and almost invisible for TEM. The XRD peaks of a second phase can appear only in the case where the coherent-scattering region for X-rays is large enough (grain size around 5 nm or larger). XRD also allows one to estimate the grain size using the peak width.

McLean wrote for the first time that the apparent solubility limit, c_{sa}, in the materials with small grain size should be above the bulk solubility limit c_s [1]. McLean calculated this difference for the grain size of 1 and 10 μm in Fe–C alloys [1]. Beke et al. discussed the grain boundary (GB) segregation-driven shift of miscibility gap in dependence on number of GB layers [2,3]. Later such a shift was observed experimentally in the Pd–H system [4]. Similar increase of the total solubility with decreasing grain size was found also for Ti and Y in alumina [5,6] and for Y and Ca in TiO_2 [7,8].

Nevertheless, the exact XRD measurements of solubility shift $c_{sa} - c_s$ in dependence on grain size d are very work intensive. Zinc oxide offers a good possibility for such investigations. ZnO is broadly used for gas sensors, as a material for varistors (doped by Bi_2O_3), and as a transparent conducting oxide in the semiconductor thin film technology. Moreover, as a possible ferromagnetic semiconductor, it is a promising material for future spintronics. According to the theoretic prediction of Dietl et al., the ZnO doped by small amounts of “magnetic” impurities like Mn or Co should possess the ferromagnetic properties [9]. This work became a starting point for the boom of experimental and theoretical works [10,11]. In the meantime several thousands papers devoted to dilute magnetic semiconductors have been published. However, the mechanisms of ferromagnetic behavior in pure and doped ZnO are far from understood. The obtained experimental results are quite contradictory. Several research groups reported the reproducible observations of ferromagnetism in ZnO. Another teams of experimentalists never succeeded to synthesize ferromagnetic ZnO. The huge interest to ferromagnetism in ZnO is because it is the cheap semiconductor which is already used in various devices and technologies. The ferromagnetic behaviour together with the attractive optical and semiconductor properties can be applied in the future in spintronics [9,10]. Recently we proposed the explanation for the contradictory results on ferromagnetism in ZnO [12]. We observed, that ferromagnetic behaviour does not appear in bulk ZnO (even doped by Mn, Co or Fe), but only in polycrystalline samples with very small grains and high specific area s_{GB} of grain boundaries. s_{GB} is the ratio of GB area to grain volume [13–16]. The ferromagnetism appears only in the case when the s_{GB} in ZnO exceeds a certain threshold called s_{th}. If s_{GB} is high enough, even the doping by “magnetic” ions is not essential, and ferromagnetism appears in pure, undoped ZnO. The viewpoint that GBs are the reason of ferromagnetism in ZnO became generally accepted in last years [10]. The presence or absence of ferromagnetism in doped ZnO critically depends on the synthesis method. Fortunately, the studies of ferromagnetism in ZnO allow the dependence of $c_{sa} - c_s$ on the grain (particle) size d to be estimated.

Therefore, the goal of this work is threefold, (1) to measure the solubility shift $c_{sa} - c_s$ in nanograined Ni-doped ZnO manufactured by the novel liquid ceramics method; (2) to analyze the $c_{sa} - c_s$ dependence on the grain size in the broad interval of d using the published data on Ni-doped ZnO [17-139]; (3) to determine the threshold value s_{th} of specific GB area for the Ni-doped zinc oxide using the published papers on its ferromagnetic behaviour [17-139].

2. EXPERIMENTAL

Pure and Ni-doped ZnO thin films consisting of dense equiaxial nanograins were produced by using the novel method of liquid ceramics [12–16]. As a precursor for the preparation of pure ZnO films, the zinc (II) butanoate diluted in the organic solvent with zinc concentrations between 1 and 4 kg/m^3 was used. In order to manufacture ZnO films doped with 5, 10, 20, 30, and 40 at.% Ni, zinc (II) butanoate solution was mixed with the nickel (II) butanoate solution in respective proportions. The butanoate precursor was deposited onto (102) single crystalline sapphire substrates and dried in air at 100 °C about 30 min. The drying was followed by thermal pyrolysis at 550 °C in air in an electrical furnace. The Zn and Ni content in doped oxides were measured by electron-probe microanalysis (EPMA) and atomic absorption spectroscopy in a Perkin-Elmer spectrometer. EPMA investigations were carried out in a Tescan Vega TS5130 MM microscope equipped by the LINK energy-dispersive spectrometer produced by Oxford Instruments. The analysis witnessed that the content of other magnetic impurities such as Mn, Co, and Fe was below 0.001 at.%. It is known from the literature [140] that the effect of a contaminated

substrate can completely conceal the ferromagnetic signal of ZnO itself. Therefore, all possible precautions were taken during the preparation procedures in order to exclude any additional ferromagnetic contaminations (for example nonmagnetic ceramic tweezers, scissors etc. were used). We carefully measured the magnetization curves for bare Al_2O_3 substrates and subtracted them from data for the substrates with deposited ZnO films. The ZnO films were transparent and sometimes with a very slight greenish furnish. They had thickness between 50 and 200 nm (determined by the edge-on TEM and EPMA). TEM investigations were carried out on a Jeol JEM–4000FX microscope at an accelerating voltage of 400 kV. XRD data were obtained on a Siemens diffractometer (Cu K_α radiation with λ = 0.154184 nm) with a secondary monochromator. Evaluation of the grain or size *D* from the x-ray peak broadening was performed using the Scherrer equation [141]. The magnetic properties were measured on a superconducting quantum interference device (Quantum Design MPMS-7 and MPMS-XL). The magnetic field was applied parallel to the sample plane ("in plane"). The diamagnetic background signals, generated by the sample holder and the substrate, were carefully subtracted, due to the small absolute magnetic moments measured in the range of 10^{-6} to 10^{-4} emu. The presence of absence of ferromagnetic properties as well as second phase NiO have been analyzed using the published papers on ferromagnetic behaviour of Ni-doped ZnO [17-139].

3. RESULTS AND DISCUSSION

Using the method of liquid ceramics we deposited the nanograined and poreless pure and Ni-doped ZnO thin films (see micrograph in Fig. 1). The mean size of equiaxial ZnO grains was about 40 nm. No visible texture can be observed in the deposited thin films: the electron diffraction rings shown in the inset in Fig. 1 are uniform without any preferred orientations of ZnO grains.

In Fig. 2a the XRD patterns are shown for the Ni-doped ZnO films containing 0, 10, 20, 30 and 40 at.% Ni. Only wurtzite lines are visible in the pure ZnO film (ICPDS Card No. 36-1451) and ZnO films containing 0, 5, and 10 at.% Ni. The peaks of the second phase, namely cubic nickel oxide NiO become visible in samples with 30 and 40 at.% Ni. Therefore, the overall solubility of Ni in ZnO fimls at 550 °C with grain size 40 nm is about 20 at.% Ni. The solubility limit in the bulk c_s is about 1.5 at.% Ni at 550 °C [24]. In Fig. 2b the dependence of lattice spacing in ZnO on Ni concentration is shown

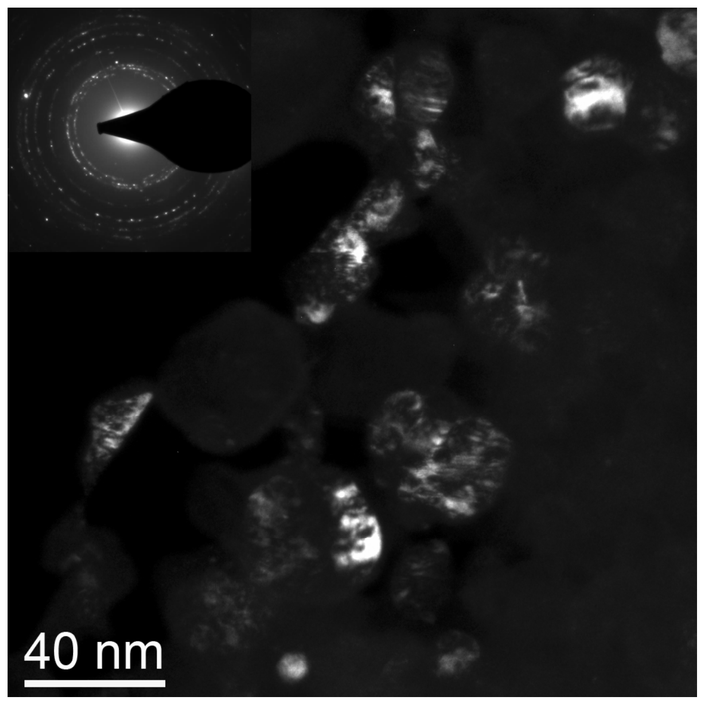

Fig. 1. Bright field TEM micrograph of the nanograined pure ZnO thin film deposited on sapphire substrate using the novel liquid ceramics method. Electron diffraction pattern (inset) shows only rings from the ZnO wurtzite structure. No texture is visible. Bright spots originate from the sapphire substrate.

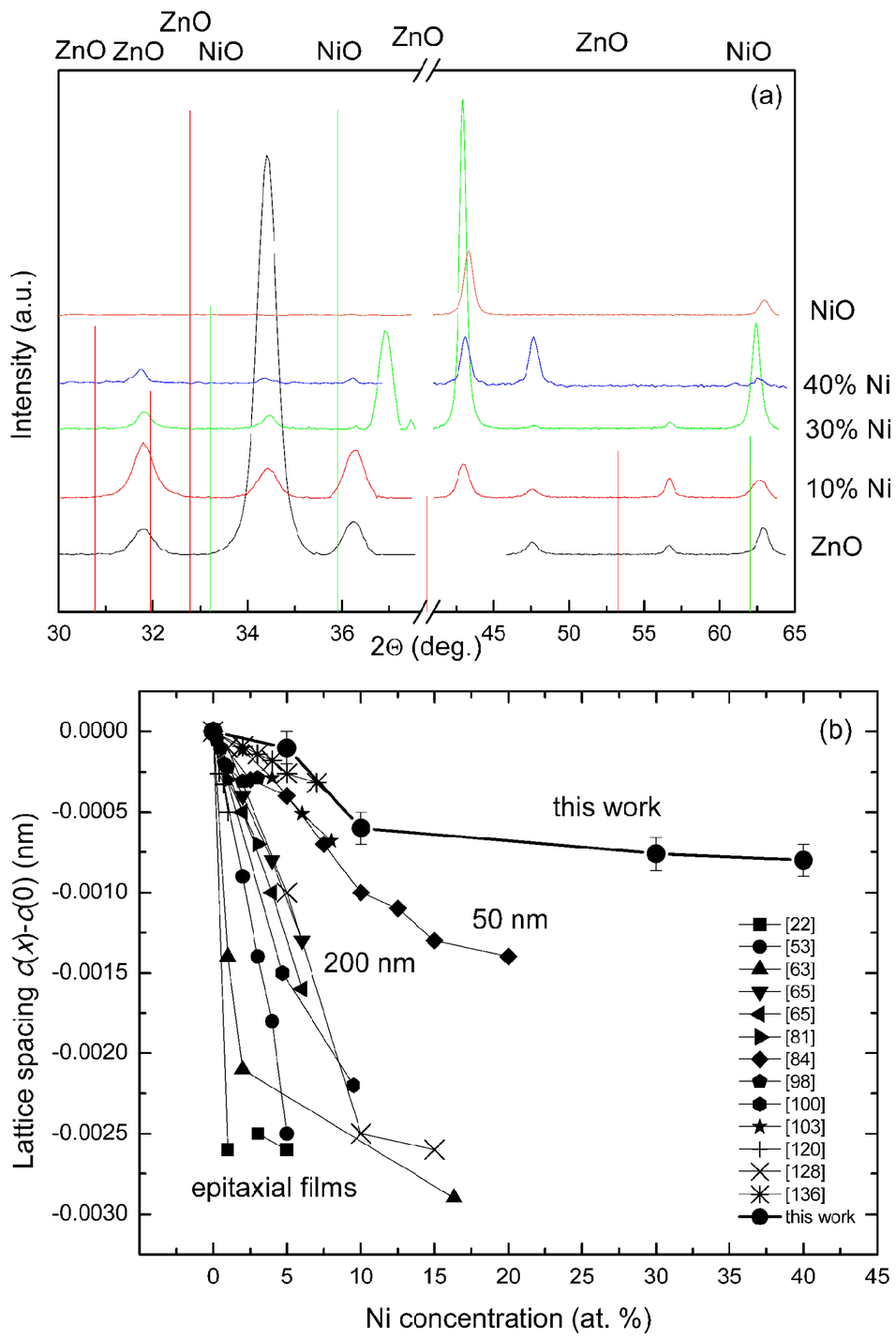

Fig. 2. (a) XRD patterns for the Ni-doped ZnO films with 0, 10, 30, 40 at.% Ni as well as for pure NiO. The positions of respective ZnO and NiO peaks are marked on the top border of a figure. (b) The decrease of lattice spacing *c* in ZnO with increasing Ni concentration for the samples with different grain size obtained by various methods [22,53,63,65, 81,84,98,100,103,120,128,136].

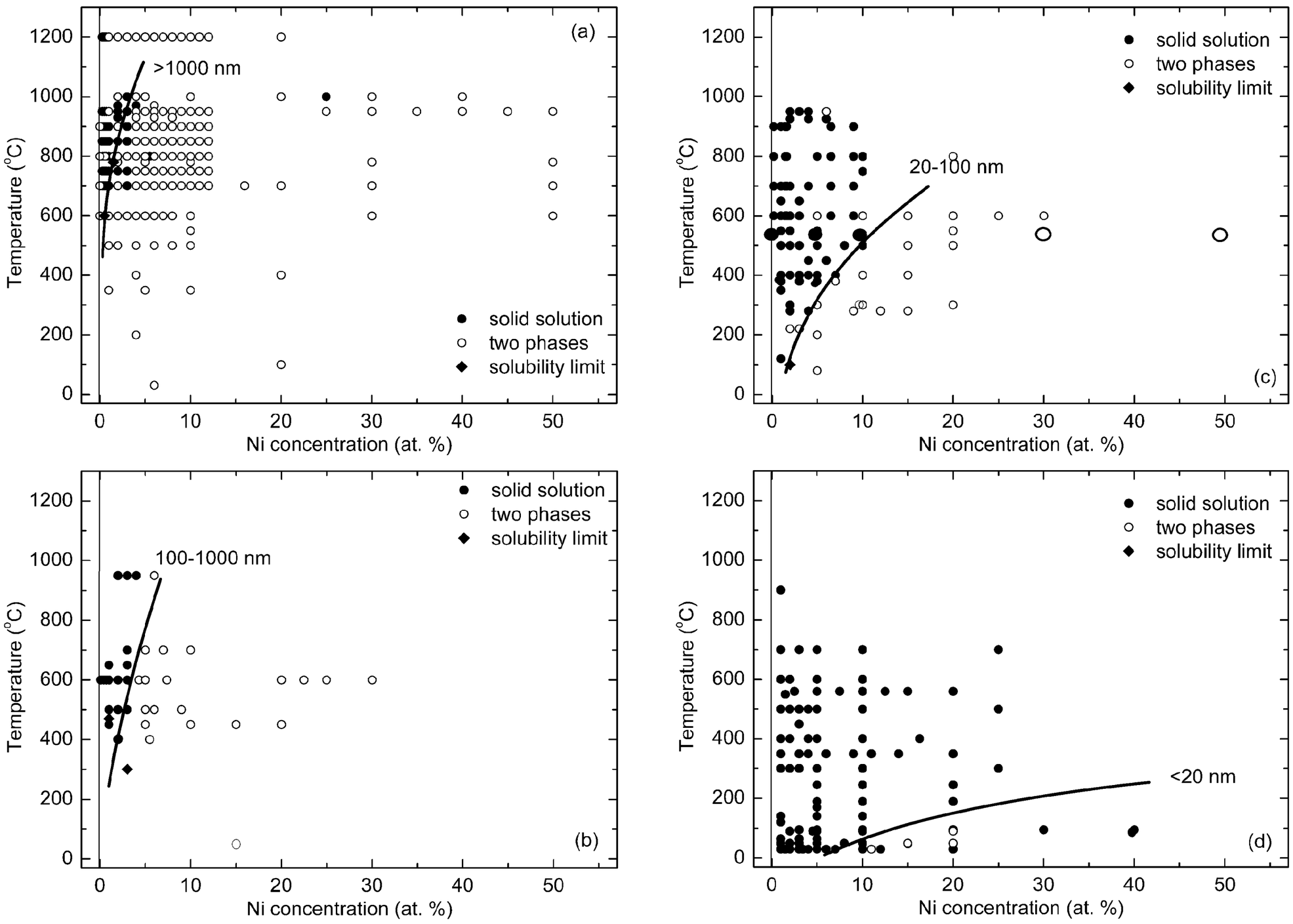

Fig. 3. Solubility limit of Ni in ZnO polycrystals with various grain size. One-phase samples containing only ZnO are shown by the filled circles. Open circles show the samples with two-phase mixture ZnO+NiO. The data obtained in this work are shown by the large circles. (a) grain size above 1000 nm [48,50,55,57,68,69,71, 79,92,98,101,109,114,115,118,119]. (b) grain size between 1000 and 100 nm [30,31,58,69,75,78,87, 90,95,104,120,130,135], (c) grain size between 100 and 20 nm [18,21,32–34,43,44,49,52,53,59,65, 69,70,76,80,83,87,88,90,91,94,96,99,127,128,132,135,137,138], (d) grain size below 20 nm [21–23,25,26, 29,35–39,41,46,47,49,51,52,54,60–64,66,67,73,74,76,83,84,86,91,93,94,97,100,110,112,113,123,126].

for the samples with different grain size obtained by various methods [17-139]. The ZnO lattice spacing decreases with increasing Ni content. This change of ZnO lattice spacing becomes slower with decreasing grain size, similar to ZnO doped by Co, Mn and Fe [13–16].

In order to find ferromagnetism in doped ZnO, it is important to ensure that it does not contain any particles of the second phase which could influence the sample's magnetic properties. In other words, it is essential that all published articles include data on the dopant concentration and presence or absence of the second phase. Usually, the presence or absence of a second phase is controlled by XRD. Measurable X-rays peaks appear in the diffraction spectra when the amount of a second phase is about 5%. TEM allows one to detect a second phase at lower content than XRD. However, such data are seldom present in the papers devoted to the magnetic behaviour of ZnO. The fact that the same method (XRD) was used to control the presence of a second phase in Ni-doped ZnO allows us to compare the data from different works and to bring them together in the same plot.

The majority of published works allows us to estimate the grain or particle size and to assign the data to a certain temperature, either that of a synthesis or that of the last thermal treatment. The published data encompass a grain (particle) size *D* of between 1 mm and 10 nm and temperatures from 300 to 1500K. This gave us the unique chance to construct the $c_{sa}(T)$ dependences for the broad interval of *D* and to compare the influence of internal boundaries and surfaces. The biggest data arrays exist for Co-, Fe- Mn and Ni-doped ZnO. The data for Co-, Fe-and Mn-doped ZnO were analysed earlier [13-16]. In this work we will analyse the Ni-doped ZnO.

In Fig. 3a the solubility (solvus) limit of Ni in ZnO polycrystals is drawn using the data on polycrystals with grain a size above 1000 nm [48,50,55,57,68,69,71,79,92,98,101,109,114,115,118,119].

The errors in Fig. 3 are below the scale of the markers. These samples were obtained by hydrothermal growth [24], autocombustion [103], sintering of conventional powders [48,68,69,79,92,98,109,114,118], Ni ion implantation into ZnO single cristals [50,55,57,71,101,115], ball milling [119]. The solubility of Ni in ZnO reaches about 4 at.% at 1000 °C and falls below 0.5 at.% at 400 °C. This line corresponds to the solubility in the volume of ZnO, the number of Ni atoms segregated in grain boundaries is negligible. In Fig. 3b the solubility (solvus) limit of Ni in ZnO polycrystals is drawn using the data on polycrystals with grain a size *D* between 1000 nm and 100 nm [30,31,58,69,75,78,87,90,95,104, 120,130,135]. These samples were obtained by the the wet chemistry deposition methods (including sol-gel method) [30,69,90,95,104,120,135], chemical pyrophoric reaction process [31], co-precipitation or sintering of nanopowders [58], spray pyrolisis [75, 78], autocombustion [87], and hydrothermal growth [130]. The solubility of Ni in ZnO (for *D* between 1000 nm and 100 nm) reaches about 8 at.% at 1000 °C and falls to 2 at.% at 400 °C.

In Fig. 3c the solubility (solvus) limit of Ni in ZnO polycrystals is drawn using the data on polycrystals with grain a size *D* between 100 nm and 20 nm [18,21,32–34,43,44,49,52,53,59,65,69,70,76,80,83, 87,88,90,91,94,96,99,127,128,132,135,137,138]. The data obtained in this work are shown by the large circles. These samples were obtained by the wet chemistry deposition methods (including sol-gel method) [32–34,44,65,76,83,90,91,94,99,127, 128,132,135], co-precipitation or sintering of nanopowders [69,88], pulsed laser deposition (PLD) [18,21,43,96], magnetron sputter deposition [49,53,138], solvothermal growth [52], Ni ion implantation into ZnO nanowires [59], spray pyrolysis [70,137], autocombustion [87,88], mechanical alloying [80]. The solubility of Ni in ZnO (for *D* between 100 nm and 20 nm) reaches about 15 at.% at 700 °C and falls to 5 at.% at 400 °C. It remains around 1 at.% even at 100 °C.

In Fig. 3d the solubility limit (solvus) of Ni in ZnO polycrystals is drawn using the data on polycrystals with grain size below 20 nm [21–23,25,26,29,35–39,41,46,47,49,51,52,54,60–64,66,67,73,74,76,83,84,86,91,93,94,97,100,110,112,113,123,126]. These samples were obtained by the wet chemistry deposition methods (including sol-gel method) [25,26,29,37,51,67,73,74,76,83,84,91,94,97,100,113,123], magnetron sputter deposition [36,39,41,49, 66,110,126], PLD [21–23,35,38,61,63,64,112], hydrothermal and solvothermal growth [46,52,60,86], Ni ion implantation into thin films [47,62,93], co-precipitation [54]. The solubility of Ni in ZnO (for $D <$ 20 nm) is very high. The two-phase mixture appears in experiments only below 200 °C. The solubility of Ni in ZnO remains around 5 at.% even at room temperature. Therefore, the Ni solubility in ZnO polycrystals strongly increases with decreasing grain size, similar to that of Co, Mn or Fe [13–16].

The quantitative estimation shows that, close to the bulk solubility limit, the thickness of a Ni-enriched layer in grain boundaries (GBs) is several monolayers. Based on the knowledge that Ni solubility depends on grain size (Fig. 3), it is possible to estimate the maximum Ni segregation in ZnO GBs. Let us calculate first the area to volume ratio for the grains and particles. If we suppose that grains and particles are spheres with diameter *D*, the surface for each particle is πD^2 and the GB area for each grain is $\pi D^2/2$ (since each GB is shared between two neighbouring grains). The volume for spherical grains and particles is the same, namely $pD^3/6$. Thus the area to volume ratio, *A*, for the free surfaces of spherical particles is $A_{FS} = 3/D$ and for GBs of spherical grains $A_{GB} = 3/2D$. One of the earliest studies of grain shape was made by Lord Kelvin in 1887 [142]. According to his work, the grain shape for optimal space-filling, is a polyhedron known as a tetrakaidecahedron. It has 14 faces, 24 corners, and 36 edges. Tetrakaidecahedrons ensure a minimal surface area and surface tension. Tetrakaidecahedron is an octahedron truncated by cube. The ratio of tetrakaidecahedron surface area to that of a sphere of the same volume is 1.099 [142]. Thus the area to volume ratio for polyhedral grains is $A_{GB} = 1.65/D$. If the ZnO GBs are covered by one monolayer (ML) of Ni, one can calculate their input, c_{GB}, in the full concentration as a product of the thickness, *t*, of a GB layer and A_{GB}. One can estimate the lattice constant of ZnO wurtzite lattice *d* as the cubic root from the unit cell volume. According to our measurements, the unit cell volume for ZnO is about 47×10^{-3} nm^3. Therefore, $d = 0.36$ nm. Thus, for the one monolayer $t = d$, $c_{GB} = d\,A_{GB} = 0.59/D$. The solubility limit of Ni in the single-crystalline or coarse-grained ZnO at 500 °C and 700°C is 1 and 2 at.% Ni, respectively (Fig. 3). If we subtract these values from the solubility limit of Ni in the fine-grained ZnO (9 and 15 at.% Ni at 500 °C and 700 °C), we obtain the GB input, c_{GB}, into total Ni solubility in the ZnO polycrystals. Thus, the experimental c_{GB} values are more than one order of magnitude higher than the calculated values for 1 ML. This fact undoubtedly indicates the multilayer GB Ni segregation in ZnO.

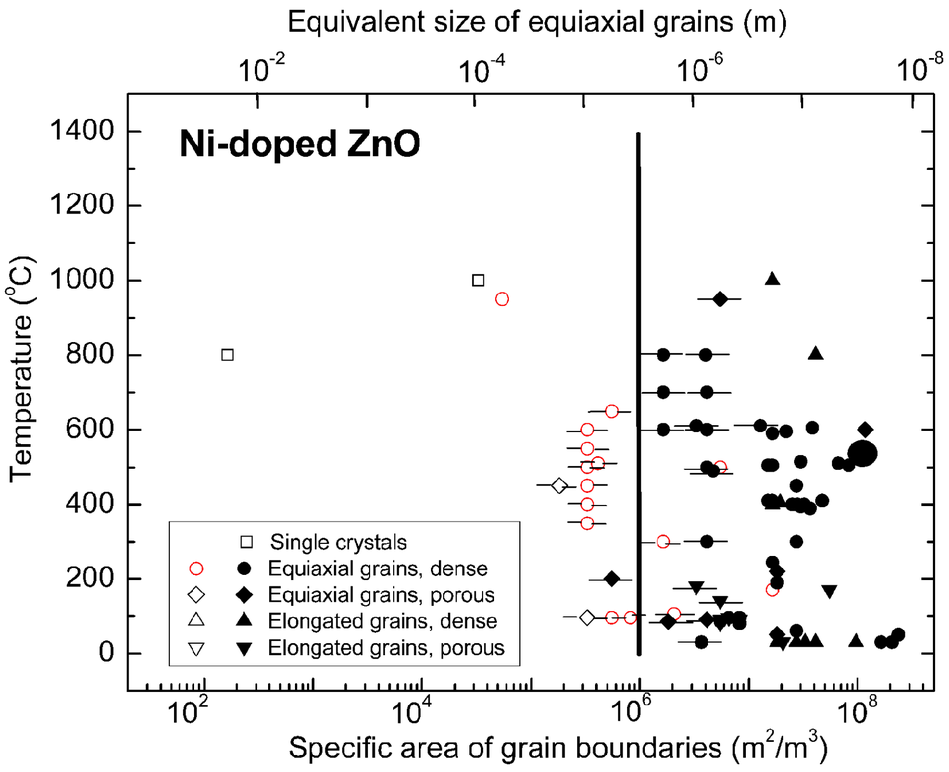

Fig. 4. FM (full symbols) and para- or diamagnetic (open symbols) behaviour of Ni-doped ZnO in dependence on the specific GB area, s_{GB}, the ratio of GB area to volume, at different preparation temperatures T. Vertical line mark the estimated threshold value s_{th}. Enlarged symbol indicate the experimental data obtained by the authors' investigations (for symbols and references see the text) [18,20,22,23,25–27,29,30,37–43,45,46–49,51,53,54,58,60–64,68,69,72,75,77,80–82,85–88,91,95,96,100,101,104,109,112,113,115,120,127,128,130–137].

The pronounced FM behaviour has been observed in our Ni-doped nanocrystalline ZnO. Dense ZnO films with 5 at.% Ni have saturation of magnetization (J_s ~ 10^{-5} emu/cm^3 above the applied field ~3 T) and hysteretic behaviour with coercivity H_c ~ 0.05 T. These magnetization and coercivity values are close to those obtained by other methods for the Ni-doped samples.

We critically analysed the published papers on the search of possible ferromagnetic behaviour in the Ni-doped ZnO [18,20,22,23,25–27,29,30,37–43,45,46–49,51,53,54,58,60–64,68,69,72,75,77,80–82,85–88,91,95,96,100,101,104,109,112,113,115,120,127,128,130–137]. The results are summarized in Fig. 4 in a T-s_{GB} plot (here T represents the annealing or synthesis temperature). They can be divided into three groups, depending on the s_{GB} value. First, the samples obtained by the magnetron and ion-beam sputter deposition or PLD having small and very small grains are almost always ferromagnetic [18,22,23,25–27,29,37–43,46–49,51,53,54,58,61,63,64,69,72,77,81,82,85,86,88,95,96,100,101,104,109,112,113,120,127,128,130–137]. The respective (filled) points are grouping in the right part of the diagram in Fig. 4. Second, the coarse-grained samples synthesised by the conventional powder sintering method, bulk single crystals or single-crystalline films are always diamagnetic or paramagnetic [40,45,68,75,80,85–88,91,101,109,115]. They are positioned in the left part of the diagram in Fig. 4. In between one finds the third group of the data, namely obtained using the samples produced by chemical vapour deposition (CVD), solution combustion or wet chemistry methods. They have intermediate properties and can be either paramagnetic or FM [20,30,60,62,63,75,82,85,86,101,109].

The diagram in Fig. 4 demonstrates that not only the pure zinc oxide [143,144] but also the Ni-doped one becomes ferromagnetic only if s_{GB} is higher than a certain crytical value s_{th}. In other words, ZnO has to contain enough GBs to become ferromagnetic. In case of Ni-doped ZnO s_{th} = (1±0.2)×10^6 m^2/m^3. This value corresponds to the grain size of about 4 μm. (If we assume that a material is fully dense and grains are equiaxial). The value of s_{th} = 1×10^6 m^2/m^3 is lower than that for pure ZnO s_{th} = 5.3×10^7 m^2/m^3 and that for Co-doped ZnO s_{th}. = 1.5×10^6 m^2/m^3. However, it is higher than that for Mn-doped ZnO s_{th} = 2.4×10^5 m^2/m^3 and Fe-doped ZnO s_{th}. = 5×10^4 m^2/m^3. It means that the addition of "magnetic" atoms to the pure ZnO drastically improved, indeed, the ferromagnetic properties of pure ZnO. Moreover, Ni improved the ferromagnetic properties of pure zinc oxide more effectively than Co. Such phenomenon, especially at high concentration of the dopant can be connected also with the GB wetting and prewetting phenomena and respective formation of thin and thick doped GB layers [145–147].

4. CONCLUSIONS

The accumulation of Ni in grain boundaries and free surfaces drastically shifts the line of Ni solubility limit in ZnO to the higher Ni concentrations. For example, at 550 °C the total solubility in the bulk is below 1 at.% Ni and in the nanograined sample with grain size below 20 nm it is above 30 at.% Ni. Thus, the phase diagrams for the materials having a grain size below 1000 nm have to be newly investigated. An especially drastic change to the phase diagrams results when the grain size is below 100 nm.

The influence of specific area of grain boundaries s_{GB} on presence or absence of ferromagnetism in Ni-doped ZnO has been analysed basing on a review of numerous research contributions from the literature towards the origin of the ferromagnetic behaviour of Ni-doped ZnO. An empirical correlation has been found that the value of the specific grain boundary area s_{GB} is the controlling factor for such

behaviour. The Ni-doped ZnO becomes ferromagnetic only if it contains enough GBs, i.e. if s_{GB} is higher than a certain threshold value s_{th}. = 1×10^6 m^2/m^3. It corresponds to the effective grain size of about 4 μm assuming a full dense material and equiaxial grains. The value of s_{th} = 1×10^6 $m^2/m^3$is lower than that for pure ZnO s_{th} = 5.3×10^7 m^2/m^3 and that for Co-doped ZnO s_{th}. = 1.5×10^6 m^2/m^3 but higher than that for Mn-doped ZnO s_{th} = 2.4×10^5 m^2/m^3 and Fe-doped ZnO s_{th}. = 5×10^4 m^2/m^3. It means that the addition of "magnetic" atoms to the pure ZnO drastically improved, indeed, the ferromagnetic properties of pure ZnO. Moreover, Ni improved the ferromagnetic properties of pure zinc oxide more effectively than Co.

ACKNOWLEDGEMENTS

The work was partially supported by the Russian Foundation for Basic Research (grants 14-48-03598, 14-42-03621, 15-03-01127, and 15-03-04220), Government of Moscow Region, Ministry of Education and Science of the Russian Federation in the framework of Increase Competitiveness Program of MISiS, European Community's Seventh Framework Programme (FP7-PEOPLE-2013-IRSES) under EC-GA no. 612552 and Karlsruhe Nano Micro Facility.

REFERENCES

[1] D. McLean, *Grain Boundaries in Metals* (Clarendon Press, Oxford, 1957).
[2] D.L. Beke, C. Cserháti, Z. Erdélyi and I.A. Szabó, *Segregation in Nanostructures, In Nanoclusters and Nanocrystals*, ed. by H.S. Nalwa (American Scientific Publishers, Valencia, CA, 2002).
[3] D.L. Beke, Z. Erdélyi, P. Bakos, C. Cserháti and I.A. Szabó, In: *Proceedings of the International Conference Solid-Solid Phase Transformations '99*, ed. by M. Koiwa, K. Otsuka and T. Miyazaki (The Japan Institute of Metals, Tokyo, 1999).
[4] J. Weissmuller and Chr. Lemier // *Phil. Mag. Lett.* **80** (2000) 411.
[5] S. Lartigue-Korinek, C. Legros, C. Carry and F. Herbst // *J. Eur. Ceram. Soc.* **26** (2006) 2219.
[6] M.A. Gülgün, R. Voytovych, I. Maclaren, M. Rühle and R.M. Cannon // *Interface Sci.* **10** (2002) 99.
[7] Q. Wang, G. Lian and E.C. Dickey // *Acta Mater.* **52** (2004) 809.
[8] C.D. Terwilliger and Y.M. Chiang // *Acta Metall. Mater.* **43** (1995) 319.
[9] T. Dietl, H. Ohno, F. Matsukura, J. Cibert and D. Ferrand // *Science* **287** (2000) 1019.
[10] T. Dietl // *Nature Mater.* **9** (2010) 965.
[11] K. Sato and H. Katayama-Yoshida // *Semicond. Sci. Technol.* **17** (2002) 367.
[12] B.B. Straumal, A.A. Mazilkin, S.G. Protasova, A.A. Myatiev, P.B. Straumal, G. Schütz, P.A. van Aken, E. Goering and B. Baretzky // *Phys. Rev. B* **79** (2009) 205206.
[13] B.B. Straumal, A.A. Mazilkin, S.G. Protasova, A.A. Myatiev, P.B. Straumal and B. Baretzky // *Acta Mater.* **56** (2008) 6246.
[14] B.B. Straumal, B. Baretzky, A.A. Mazilkin, S.G. Protasova, A.A. Myatiev and P.B. Straumal // *J. Eur. Ceram. Soc.* **29** (2009) 1963.
[15] B.B. Straumal, S.G. Protasova, A.A. Mazilkin, P.B. Straumal, G. Schütz, Th. Tietze, E. Goering and B. Baretzky // *Beilstein J. Nanotechnol.* **4** (2013) 361.
[16] S.G. Protasova, B.B. Straumal, A.A. Mazilkin, S.V. Stakhanova, P.B. Straumal and B. Baretzky // *J. Mater. Sci.* **49** (2014) 4490.
[17] J.B. Cui and U. J. Gibson // *Appl. Phys. Lett.* **87** (2005) 133108.
[18] L.S. Dorneles, D. O'Mahony, C.B. Fitzgerald, F. McGee, M. Venkatesan, I. Stanca, J.G. Lunney and J.M.D. Coey // *Appl. Surf. Sci.* **248** (2005) 406.
[19] G. Peia, C. Xia, S. Cao, J. Zhang, F. Wu and J. Xu // *J. Magn. Magn. Mater.* **302** (2006) 340.
[20] K. Ueda, H. Tabata and T. Kawai // *Appl. Phys. Lett.* **79** (2001) 988.
[21] K. Ando, H. Saito, Z. Jin, T. Fukumura, M. Kawasaki, Y. Matsumoto and H. Koinuma // *J. Appl. Phys.* **89** (2001) 7284.
[22] T. Wakano, N. Fujimura, Y. Morinaga, N. Abe, A. Ashida and T. Ito // *Phys. E* **10** (2001) 260.
[23] M. Venkatesan, C.B. Fitzgerald, J.G. Lunney and J.M.D. Coey // *Phys. Rev. Lett.* **93** (2004) 177206.
[24] C.H. Bates, W.B. White and R. Roy // *J. Inorg. Nucl. Chem.* **28** (1966) 397.
[25] O. Perales-Perez, A. Parra-Palomino, R. Singhal, P.M. Voyles, Y. Zhu, W. Jia and M. S. Tomar // *Nanotechnol.* **18** (2007) 315606.
[26] G.J. Huang, J.B. Wang, X.L. Zhong, G.C. Zhou and H.L. Yan // *J. Mater. Sci.* **42** (2007) 6464.

[27] H. Wang, Y. Chen, H.B. Wang, C. Zhang, F.J. Yang, J.X. Duan, C.P. Yang, Y.M. Xu, M.J. Zhou and Q. Li // *Appl. Phys. Lett.* **90** (2007) 052505.
[28] S. Zhou, K. Potzger, G. Zhang, F. Eichhorn, W. Skorupa, M. Helm and J. Fassbender // *J. Appl. Phys.* **100** (2006) 114304.
[29] C.J. Cong, J.H. Hong, Q.Y. Liu, L. Liao and K.L. Zhang // *Sol. State Comm.* **138** (2006) 511.
[30] B.B. Li, X.Q. Xiu, R. Zhang, Z.K. Tao, L. Chen, Z.L. Xie, Y.D. Zheng and Z. Xie // *Mater. Sci. Semicond. Proc.* **9** (2006) 141.
[31] S.K. Mandal, A.K. Das, T.K. Nath and D. Karmakar // *Appl. Phys. Lett.* **89** (2007) 144105.
[32] B.B. Li, X.Q. Xiu, R. Zhang, Z.K. Tao, L. Chen, Z.L. Xie, Y.D. Zheng and B. He // *Chinese Phys. Lett.* **23** (2006) 907.
[33] S. Thota, T. Dutta and J. Kumar // *J. Phys. Cond. Mat.* **18** (2006) 2473.
[34] V.A. Chitta, J.A. H. Coaquira, J.R.L. Fernandez, C.A. Duarte, J.R. Leite, D. Schikora, D.J. As, K. Lischka and E. Abramof // *Appl. Phys. Lett.* **85** (2004) 3777.
[35] X. Liu, F. Lin, L. Sun, W. Cheng, X. Ma and W. Shi // *Appl. Phys. Lett.* **88** (2006) 062508.
[36] Z. Yin, N. Chen, F. Yang, S. Song, C. Chai, J. Zhong, H. Qian and K. Ibrahim // *Sol. State Comm.* **135** (2005) 430.
[37] D.A. Schwartz, K.R. Kittilstved and D.R. Gamelin // *Appl. Phys. Lett.* **85** (2004) 1395.
[38] M. Snure, D. Kumar and A. Tiwari // Appl. Phys. Lett. **94** (2009) 012510.
[39] X.J. Liu, X.Y. Zhu, C. Song, F. Zeng and F. Pan // *J. Phys. D: Appl. Phys.* **42** (2009) 035004.
[40] T.L. Phan, R. Vincent, D. Cherns, N.X. Nghia and V.V. Ursaki // *Nanotechnol.* **19** (2008) 475702.
[41] B. Pandey, S. Ghosh, P. Srivastava, D.K. Avasthi, D. Kabiraj and J.C. Pivin // *J. Magn. Magn. Mater.* **320** (2008) 3347.
[42] X.L. Zhang, R. Qiao, J.C. Kim and Y.S. Kang // *Crystal Growth & Design* **8** (2008) 2609.
[43] W. Yu, L.H. Yang, X.Y. Teng, J.C. Zhang, Z.C. Zhang, L. Zhang and G.S. Fu // *J. Appl. Phys.* **103** (2008) 093901.
[44] S. Singh, N. Rama, K. Sethupathi and M.S. Ramachandra Rao // *J. Appl. Phys.* **103** (2008) 07D108.
[45] J. Alaria, M. Venkatesan and J.M.D. Coey // *Appl. Phys.* **103** (2008) 07D123.
[46] C. Cheng, G. Xu, H. Zhang and Y. Luo // *Mater. Lett.* **62** (2008) 1617.
[47] S. Ghosh, D. Kanjilal, B. Pandey, M. Saurav and P. Kumar // *Radiat. Eff. Def. Sol.* **163** (2008) 215.
[48] X. Mao, W. Zhong and Y. Du // *J. Magn. Magn. Mater.* **320** (2008) 1102.
[49] E. Liu, P. Xiao, J.S. Chen, B.C. Lim and L. Li // *Curr. Appl. Phys.* **8** (2008) 408.
[50] S. Zhou, K. Potzger, J. von Borany, R. Grötzschel, W. Skorupa, M. Helm and J. Fassbender // *Phys. Rev. B* **77** (2008) 035209.
[51] K.C. Barick, M. Aslam, J. Wu, V.P. Dravid and D. Bahadur // *J. Mater. Res.* **24** (2009) 3543.
[52] W. Lojkowski, A. Gedanken, E. Grzanka, A. Opalinska, T. Strachowski, R. Pielaszek, A. Tomaszewska-Grzeda, S. Yatsunenko, M. Godlewski, H. Matysiak and K.J. Kurzydłowski // *J. Nanopart. Res.* **11** (2009) 1991.
[53] D.-L. Hou, R.-B. Zhao, Y.-Y. Wei, C.-M. Zhen, C.-F. Pan and G.-D. Tang // *Curr. Appl. Phys.* **10** (2010) 124.
[54] P.K. Sharma, R.K. Dutta and A.C. Pandey // *J. Magn. Magn. Mater.* **321** (2009) 3457.
[55] M. Schumm, M. Koerdel, S. Müller, C. Ronning, E. Dynowska, Z. Gołacki, W. Szuszkiewicz and J. Geurts // *J. Appl. Phys.* **105** (2009) 083525.
[56] K. Potzger and S. Zhou // *Phys. Status Solidi B* **246** (2009) 1147.
[57] S. Zhou, K. Potzger, Q. Xu, G. Talut, M. Lorenz, W. Skorupa, M. Helm, J. Fassbender, M. Grundmann and H. Schmidt // *Vacuum* **83** (2009) S13.
[58] M. El-Hilo, A.A. Dakhel and A.Y. Ali-Mohamed // *J. Magn*. *Magn. Mater.* **321** (2009) 2279.
[59] S. Müller, M. Zhou, Q. Li and C. Ronning // *Nanotechnol.* **20** (2009) 135704.
[60] Y. Zuo, S. Ge, Z. Chen, L. Zhang, X. Zhou and S. Yan // *J. Alloys Compd.* **470** (2009) 47.
[61] X. Huang, G. Li, B. Cao, M. Wang and C. Hao // *J. Phys. Chem. C* **113**(2009) 4381.
[62] B. Pandey, S. Ghosh, P. Srivastava, P. Kumar and D. Kanjilal // *J. Appl. Phys.* **105** (2009) 033909.
[63] S. Thota, L.M. Kukreja and J. Kumar // *Thin Solid Films* **517**(2008) 750.
[64] J.C. Pivin, G. Socol, I. Mihailescu, P. Berthet, F. Singh, M.K. Patel and L. Vincent // *Thin Solid Films* **517** (2008) 916.

[65] C.K. Ghosh, S. Malkhandi, M.K. Mitra and K.K. Chattopadhyay // *J. Phys.D: Appl. Phys.* **41** (2008) 245113.
[66] S. Ghosh, P. Srivastava, B. Pandey, M. Saurav, P. Bharadwaj, D.K. Avasthi, D. Kabiraj and S.M. Shivaprasad // *Appl. Phys. A* **90**(2008) 765.
[67] D.M. Fernandes, A.A. Winkler Hechenleitner, M.F. Silva, M.K. Lima, P.R. Stival Bittencourt, R. Silva, M.A. Custódio Melo and E.A. Gómez Pineda // *Mater. Chem. Phys.* **118** (2009) 447.
[68] G. Srinet, R. Kumar and V. Sajal // *Ceram. Internat.* **39** (2013) 7557.
[69] G. Srinet, R. Kumar and V. Sajal // *J. Appl. Phys.* **114** (2013) 033912.
[70] S.C. Das, R.J. Green, J. Podder, T.Z. Regier, G.S. Chang and A. Moewes // *J. Phys. Chem. C* **117** (2013) 12745.
[71] R.P. Borges, B. Ribeiro, M.M. Cruz, M. Godinho, U. Wahl, R.C. da Silva, A.P. Gonçalves and C. Magén // *Eur. Phys. J. B* **86** (2013) 254.
[72] F. Ahmed, N. Arshi, M.S. Anwar, R. Danish and B.H. Koo // *J. Korean Phys. Soc.* **62** (2013) 1479.
[73] J.K. Salem, T.M. Hammad and R.R. Harrison // *J. Mater. Sci.: Mater. Electron.* **24** (2013) 1670.
[74] S. Mondal and P. Mitra // *Ind. J. Phys.* **87** (2013) 125.
[75] E. Chikoidze, M. Boshta, M.H. Sayed and Y. Dumont // *J. Appl. Phys.* **113** (2013) 043713.
[76] L. Arda, M. Açýkgöz and A. Güngör // *J. Supercond. Novel Magnet.* **25** (2012) 2701.
[77] S.H. Chiu, H.S. Hsu and J.C. A. Huang // *IEEE Trans. Magn.* **48** (2012) 3933.
[78] N.L. Tarwal, P.S. Shinde, Y.W. Oh, R.C. Korošec and P.S. Patil // *Appl. Phys. A* **109** (2012) 591.
[79] Z.-Y. Chen, Z.Q. Chen, B. Zou, X.G. Zhao, Z. Tang and S.J. Wang // *J. Appl. Phys.* **112** (2012) 083905.
[80] M. Bououdina, N. Mamouni, O. M. Lemine, A. Al-Saie, A. Jaafar, B. Ouladdiaf, A. El Kenz, A. Benyoussef and E.K. Hlil // *J. Alloys Compd.* **536** (2012) 66.
[81] F. Ahmed, N. Arshi, M.S. Anwar, S.H. Lee, E.S. Byon, N.J. Lyu and B.H. Koo // *Curr. Appl. Phys.* **12** (2012) S174.
[82] S.H. Chiu and J.C.A. Huang // *J. Non-Cryst. Sol.* **358** (2012) 2453.
[83] G. Murugadoss // *J. Mater. Sci. Technol.* **28** (2012) 587.
[84] D. Hu, Y.J. Liu, H.S. Li, X.Y. Cai, X.L. Yan and Y.D. Wang // *Mater. Technol.* **27** (2012) 243.
[85] S. Zhao, P. Li and Y. Wie // *Powder Technol.* **224** (2012) 390.
[86] R. Varadhaseshan and S.M. Sundar // *Appl. Surf. Sci.* **258** (2012) 7161.
[87] J. Mohapatra, D.K. Mishra and S.K. Singh // *Mater. Lett.* **75** (2012) 91.
[88] M. Saleem, S. Atiq, S. Naseem and S.A. Siddiqi // *J. Korean Phys. Soc.* **60** (2012) 1772.
[89] R. Saravanan, K. Santhi, N. Sivakumar, V. Narayanan and A. Stephen // *Mater. Character.* **67** (2012) 10.
[90] A.K. Zak, W.H.A. Majid, M.E. Abrishami, R. Yousefi and R. Parvizi // *Sol. State Sci.* **14** (2012) 488.
[91] A.P. Vijayaparkavi and S. Senthilkumaar // *J. Supercond. Novel Magnet.* **25** (2012) 427.
[92] A. Ekicibil, G. Bulun, S. K. Çetin, Z. Dikmen, Ö. Orhun, T. Firat and K. Kiymaç // *J. Supercond. Novel Magnet.* **25** (2012) 435.
[93] P. Srivastava, S. Ghosh, B. Joshi, P. Satyarthi, P. Kumar, D. Kanjilal, D. Buerger, S. Zhou, H. Schmidt, A. Rogalev and F. Wilhelm // *J. Appl. Phys.* **111** (2012) 013715.
[94] M. E. Ghazi, M. Izadifard, F. Esmaili Ghodsi and M. Yuonesi // *J. Supercond*. *Novel Magnet.* **25** (2012) 101.
[95] R.N. Aljawfi and S. Mollah // *J. Magn. Magn. Mater.* **323** (2011) 3126.
[96] C. Jin, R. Aggarwal, W. Wei, S. Nori, D. Kumar, D. Ponarin, A.I. Smirnov, J. Narayan and R.J. Narayan // *Metal. Mater. Trans. A* **42** (2011) 3250.
[97] X. Yan, D. Hu, H. Li, L. Li, X. Chong and Y. Wang // *Phys. B* **406** (2011) 3956.
[98] H. Çolak and O. Türkoğlu // *J. Mater. Sci. Technol.* **27** (2011) 944.
[99] A. Yildiz, B. Kayhan, B. Yurduguzel, A.P. Rambu, F. Iacomi and S. Simon // *J. Mater. Sci.: Mater. Electron.* **22** (2011) 1473.
[100] I. Balti, A. Mezni, A. Dakhlaoui-Omrani, P. Léone, B. Viana, O. Brinza, L.-S. Smiri and N. Jouini // *J. Phys. Chem. C* **115** (2011) 15758.
[101] C. Okay, B.Z. Rameev, S. Güler, R.I. Khaibullin, R.R. Khakimova, Y.N. Osin, N. Akdoğan, A.I. Gumarov, A. Nefedov,

H. Zabel and B. Aktaş // *Appl. Phys. A* **104** (2011) 667.
[102] A.A. M. Farag, M. Cavaş, F. Yakuphanoglu and F.M. Amanullah // *J. Alloys Compd.* **509** (2011) 7900.
[103] R. Elilarassi and G. Chandrasekaran // *J. Mater. Sci.: Mater. Electron.* **22** (2011) 751.
[104] J. Mohapatra, D.K. Mishra, S.K. Kamilla, V.R.R. Medicherla, D.M. Phase, V. Berma and S. K. Singh // *Phys. Status Solidi B* **248** (2011) 1352.
[105] R.K. Singhal, S. Kumar, Y.T. Xing, U.P. Deshpande, T. Shripathi, S.N. Dolia, and E. Saitovitch // *Mater. Lett.* **65** (2011) 1485.
[106] Y. Liu, T. Wang, X. Sun, Q. Fang, Q. Lu, X. Song and Z. Sun // *Appl. Surf. Sci.* **257** (2011) 6540.
[107] M. Yu, H. Qiu, X. Chen, H. Li and W. Gong // *Mater. Chem. Phys.* **126** (2011) 797.
[108] Z. Liu, Q. Zhang, G. Shi, Y. Li and H. Wang // *J. Magn. Magn. Mater.* **323** (2011) 1022.
[109] R.K. Singhal, S.C. Sharma, P. Kumari, S. Kumar, Y.T. Xing, U.P. Deshpande, T. Shripathi and E. Saitovitch // *J. Appl. Phys.* **109** (2011) 063907.
[110] J. J. Lu, T.C. Lin, S.Y. Tsai, T.S. Mo and K.J. Gan // *J. Magn. Magn. Mater.* **323** (2011) 829.
[111] J. Das, D.K. Mishra, D.R. Sahu and B.K. Roul // *Mater. Lett.* **65** (2011) 598.
[112] X. Wang, L. Zhu, L. Zhang, J. Jiang, Z. Yang, Z. Ye and B. He // *J. Alloys Compd.* **509** (2011) 3282.
[113] K. Srinivas, S.M. Rao and P.V. Reddy // *J. Nanopart. Res.* **13** (2011) 817.
[114] K.S. Syed Ali, R. Saravanan and M. Açikgöz // *Cryst. Res. Technol.* **46** (2011) 41.
[115] R.P. Borges, B. Ribeiro, A.R.G. Costa, C. Silva, R.C. da Silva, G. Evans, A.P. Gonçalves, M.M. Cruz and M. Godinho // *Eur. Phys. J. B* **79** (2011) 185.
[116] K.C. Sebastian, M. Chawda, L. Jonny and D. Bodas // *Mater. Lett.* **64** (2010) 2269.
[117] Y. Saeed, S. Nazir, A.H. Reshak and A. Shaukat // *J. Alloys Compd.* **508** (2010) 245.
[118] V. Goyal, K.P. Bhatti and S. Chaudhary // *J. Alloys Compd.* **508** (2010) 419.
[119] F. Gao, J. Zhzao and K. Wu // *J. Wuhan Univ. Technol. Mater. Sci.* **25** (2010) 770.
[120] R.B. Zhao, D.L. Hou, J.M. Guo,·C.M. Zhen and G. D. Tang // *J. Supercond. Novel Magnet.* **23** (2010) 1261.
[121] K.C. Barick, S. Singh, M. Aslam and D. Bahadur // *Micropor. Mesopor. Mater.* **134** (2010) 195.
[122] M. Yu, H. Qiu and X. Chen // *Thin Solid Films* **518** (2010) 7174.
[123] Y. Zhang, E.-W. Shi and Z.-Z. Chen // *Mater. Sci. Semicond. Proc.* **13** (2010) 132.
[124] T. Singh, T.J. Mountziaris and D. Maroudas // *Appl. Phys. Lett.* **97** (2010) 073120.
[125] Z. Yu, S. Ge, Y. Zuo, G. Wang and F. Zhang // *Appl. Surf. Sci.* **256** (2010) 5813.
[126] S.M. Zhou, H.L. Yuan, L.S. Liu, X.L. Chen, S.Y. Lou, Y.M. Hao, R.J. Yuan and N. Li // *Nanosc. Res. Lett.* **5** (2010) 1284.
[127] L.-N. Tong, T. Cheng, H.-B. Han, J.-L. Hu, X.-M. He, Y. Tong and C.M. Schneider // *J. Appl. Phys.* **108** (2010) 023906.
[128] L.-N. Tong, X.-M. He, H.-B. Han, J.-L. Hu, A.-L. Xia and Y. Tong // *Sol. State Comm.* **150** (2010) 1112.
[129] E.S. Kumar, S. Venkatesh and M.S. Ramachandra Rao // *Appl. Phys. Lett.* **96** (2010) 232504.
[130] C. Xia, C. Hu, Y. Tian, B. Wan, J. Xu and X. He // *Phys. E* **42** (2010) 2086.
[131] J. Anghel, A. Thurber, D.A. Tenne, C.B. Hanna and A. Punnoose // *J. Appl. Phys.* **107** (2010) 09E314.
[132] A. Singhal, S. N. Achary, J. Manjanna, S. Chatterjee, P. Ayyub and A.K. Tyagi // *J. Phys. Chem. C* **114** (2010) 3422.
[133] J.M. Wesselinowa and A.T. Apostolov // *J. Appl. Phys.* **107** (2010) 053917.
[134] L. Wang, Z. Xu, F. Zhang, L. Lu and X. Xu // *J. Nanosci. Nanotechnol.* **10** (2010) 1852.
[135] X.J. Ye, H.A. Song, W. Zhong, X.S. Qi, M.H. Xu, C.Q. Jin, Z.X. Yang, C.T. Au and Y.W. Du // *Sci. China: Technol. Sci.* **53** (2010) 293.
[136] D.-L. Hou, R.-B. Zhao, Y.-Y. Wei, C.-M. Zhen, C.-F. Pan and G.-D. Tang // *Curr. Appl. Phys.* **10** (2010) 124.
[137] M. Subramanian, F.-Y. Ran, M. Tanemura, T. Hihara, T. Soga and T. Jimbo // *Jap. J. Appl. Phys.* **49** (2010) 06GJ02.
[138] S.M. Zhou, H.L. Yuan, L.S. Liu, X.L. Chen, S.Y. Lou, Y.M. Hao, R.J. Yuan and N. Li // *Nanoscale Res. Lett.* **5** (2010) 1284.
[139] R.N. Gayen, A. Rajaram, R. Bhar and A.K. Pal // *Thin Solid Films* **518** (2010) 1627.
[140] Y. Belghazi, G. Schmerber, S. Colis, J.L. Rehspringer and A. Dinia // *Appl. Phys. Lett.* **89** (2006) 122504.
[141] J.L. Lábár // *Microsc. Microanal.* **14** (2008) 287.

[142] W.F. Hosford, *Materials Science: An Intermediate Text* (Cambridge University Press; Cambridge etc., 2007).
[143] B.B. Straumal, A.A. Mazilkin, S.G. Protasova, A.A. Myatiev, P.B. Straumal, E. Goering and B. Baretzky // *Phys. Stat. Sol. B* **248** (2011) 581.
[144] Th. Tietze, P. Audehm, Y.C. Chen, G. Schütz, B.B. Straumal, S.G. Protasova, A.A. Mazilkin, P.B. Straumal, Th. Prokscha, H. Luetkens, Z. Salman, A. Suter, B. Baretzky, K. Fink, W. Wenzel, D. Danilov and E. Goering // *Sci. Rep.* **5** (2015) 8871.
[145] L.-S. Chang, C.-H. Yeh and B.B. Straumal // *Rev. Adv. Mater. Sci.* **21** (2009) 1.
[146] A.S. Gornakova, B.B. Straumal, S. Tsurekawa, L.-S. Chang and A.N. Nekrasov // *Rev. Adv. Mater. Sci.* **21** (2009) 18.
[147] B.B. Straumal, A.A. Mazilkin, S.G. Protasova, A.M. Gusak, M.F. Bulatov, A.B. Straumal and B. Baretzky // *Rev. Adv. Mater. Sci.* **38** (2014) 17.